The effect of friction and impact angle on the spermatozoa–oocyte local contact dynamics
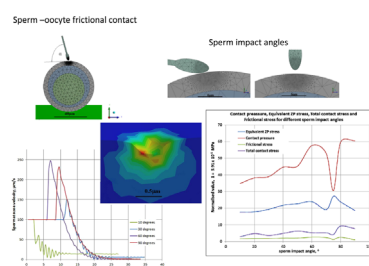
Andjelka Hedrih [a,*], Milan Banić [b]

[a] Department for Bio-Medical Science, State University of Novi Pazar, Vuka Karadzica bb, 36 300 Novi Pazar, Serbia
[b] Department for Mechanical Design, Development and Engineering, Mechanical Engineering Faculty, University of Nis, Aleksandra Medvedeva 14, 18000 Nis, Serbia

HIGHLIGHTS

- Sperm–oocyte local contact dynamics are studied trough biomechanical FEM analysis.
- Sperm–oocyte contact was defined as non-linear frictional contact.
- Deformations of ZP relative to different sperm impact angles (SIA) are discussed.
- An effect which resembles the "slip-stick" effect was identified.
- Favorable ZP-stress state for sperm penetration for different SIA are discussed.

GRAPHICAL ABSTRACT

ABSTRACT

Although a large proportion of biomolecules involved in spermatozoa–oocyte interaction has been discovered so far, many details of fertilization mechanism remain unknown. Both biochemical and biomechanical components exist in the fertilization process. Mammalian sperm evolved a ZP (zona pelucida) thrust reduction penetration strategy probably in response to the ZP resilient elasticity.

Using a biomechanical approach and FEM analysis, local contact stress, ZP deformations during impact and attempt of sperm head penetration relative to different sperm impact angles (SIA) were studied. The sperm–oocyte contact was defined as non-linear frictional contact. A transient structural analysis at 37 °C revealed that, from the mechanical standpoint there are SIA that are more favorable for possible ZP penetration due to larger equivalent stress of ZP. An "slip-stick" resembling effect was identified for almost all examined SIA. The sperm head–ZP contact area increases as SIA decreases. Favorable ZP-stress state for sperm penetration regarding SIA are discussed.

© 2016 Elsevier Ltd. All rights reserved.

1. Introduction

Fertilization process in mammals is a complex multiphase process that requires healthy oocyte and certain amount of functional spermatozoa. Classical concept of fertilization includes binding of spermatozoa to a 3D mesh-like extracellular structures of the oocyte–Zona pellucida (ZP) (Familiari et al., 2006; Martinova et al., 2008), the acrosome reaction and subsequent penetration of spermatozoa through ZP, binding and fusion of a spermatozoid with the oolemma, activation of the oocyte–cortical reaction, releasing the contents of the cortical vesicles into the perivitelline space and polyspermy block-consequent prevention of other

* Correspondence to: Trg Ucitelj Tase 3/9, 18 000 Nis, Serbia.
Tel.: +381 64 801 33 20; fax: +381 18 42 41 663.
E-mail addresses: handjelka@hm.co.rs, handjelka@gmail.com (A. Hedrih).

spermatozoa to fertilizing the oocyte (Talbot et al., 2003; Okabea and Cummins, 2007; Gaffney et al., 2011; Gadella, 2013).

During their chemotactical, rheotactical and thermotactical (Miki and Clapham, 2013) movement in female reproductive tract some spermatozoa will pass through complex metabolic and structural changes, becoming fertilization-competent. (Flesch and Gadella, 2000). Only a small fraction of a given sperm population (averaging around 10%) is responsive to different factors released from female reproductive tract and these represent capacitated spermatozoa (Eisenbach, 1999).

Sperm swimming velocity is a key determinant of male fertilization success (Malo et al., 2006). Mouse spermatozoa, as very vulnerable cells, develop strategies to survive long enough to reach and fertilize the oocytes. Spermatozoa of species with multiple partners mating system develop strategies to increase fertilization success by increasing the sperm swimming velocity by acquiring more energy for movements (longer midpiece, or longer flagella) (Anderson and Dixson, 2002; Firman and Simmons, 2010; Tourmente et al., 2011)

According to the classical fertilization concept, recognition and binding of spermatozoa to ZP will cause the acrosome reaction and consequent release of acrosome enzymes that will digest the ZP and ease the sperm penetration through it. Bedford (1998) argues that sperm penetration of ZP is only lytic event and that has also a biomechanical component that precludes lytic events.

When a spermatozoa fuse with oolema, ZP changes its structure and biomechanical properties – it becomes harder and resistant not only to proteolysis but also to mechanical forces (Sun et al., 2003; Papi et al., 2009).

Different computational techniques are used for modeling biological processes in reproductive system. Boundary element method for motion of a micromachine with a head and an elastic tail immersed in viscous media (Nasseri and Phan-Thien, 1997a, 1997b) could be applicable for sperm motion in viscous fluid with some limitations; finite element model to simulate multiple morphogenetic movements of a simplified ellipsoidal Drosophila embryo (Allena et al., 2010). To parametrize shell-like deformations inside membrane of Drosophila embryo a technique described by (Allena and Aubry, 2011) could be used. Finite element method is also used in characterization of vibration properties of mouse embryo (Hedrih and Ugrcic, 2013).

There several biomechanial models of fertilization proces that are based on sperm–egg interaction (Gefen, 2010; Kozlovsky and Gefen, 2012, 2013; Hedrih et al., 2013, 2015). First three are based on contact mechanics and other two are oscillatory models.

Using contact mechanics based modeling Gefen (2010) modeled relationship between sperm velocity and pressures applied to the ZP during early sperm–oocyte penetration. The analysis showed that sperm velocity has higher impact on pressure generated on the ZP surface than sperm head density. Kozlovsky and Gefen (2012) predicted that during the early stage of penetration into the ZP, biochemical binding forces acting on spermatozoa, are smaller than the mechanically-generated propulsive forces. "Hyperactivation of the spermatozoid and the sharpness of the spermatozoid head are all important factors that govern successful sperm penetration into the ZP" (Kozlovsky and Gefen, 2013). According to their analysis ZP hardening process as well as ZP thickness had a negligible effect on the maximum contact pressures, and the maximum penetration of the head of the spermatozoon.

Boccaccio et al. (2012) developed a hybrid procedure to investigate the biomechanical behavior of ZP membranes extracted from mature and fertilized bovine oocytes. The authors developed new hybrid model in order to increase the understanding of mechanisms that may lead to the biomechanical hardening of ZP, as well as to determine it's elastic properties. The hybrid model combines atomic force microscopy (AFM) nanoindentation measurements, nonlinear finite element analysis and nonlinear optimization algorithms. The displacement values measured by AFM nanoindentation measurements were compared with the corresponding results of FE analysis. The optimization algorithm was defined in order to extract parameters of material model for which there is a matching of experimental and FE data. Authors used three widely used hyperplastic models: Mooney–Rivlin, neo-Hookean and Arruda–Boyce eight-chain model for a constitutive model of the ZP. During FE modeling, Boccaccio et al. (2012) used axisymmetric finite element (FE) model: blunt conical indenter was treated as a rigid body and the ZP membrane was modeled as incompressible hyperelastic slab with 60 μm diameter and 10 μm thickness. Contact between AFM tip and ZP was assumed to be frictionless and analysis accounted for nonlinearity due to large deformations. During analysis the authors established that the hyperelastic behavior of the ZP membrane was always driven mainly by shear modulus, regardless of the constitutive model considered. Moreover, they established that the Arruda–Boyce model showed best results in capturing the biomechanical behavior of the ZP.

The strain-hardening behavior of an incompressible ZP membrane in AB model is predicted by using two constants: the shear modulus and the distensibility. Non-linear optimization softer compare results of computed force-indentation curves in FE analysis with experimental data, computed the error function and perturbed material parameters to minimize the error. Using this method they extract the elastic parameters of ZP membrane by using formulation of the inverse problem (Boccaccio et al., 2012). The qualitative results of Boccaccio et al. (2012) are in concordance with previous results that ZP gets harder upon fertilization and the inner ZP layer is harder compare to outer ZP layer in fertilized oocyte that is in concordance with ultra-structural experiments that inner ZP layers have more densely packed ZP glycoproteins (Martinova et al., 2008). The value of this paper is in hybrid procedure, FE model of ZP that is adequate for AFM probing experiments they used and usage of AB eight chain model instead of modified Hertzian model.

Using the same hybrid procedure (nonlinear FE analysis and nonlinear optimization) Boccaccio et al. (2014) developed optimization-based algorithm for extracting ZP linear viscoelastic properties in experiments with ZP of mature porcine oocyte: shear modulus, distensibility, Prony constant and relaxation time constant. The first two parameters describe the hyperelastic properties of ZP and the second two the viscous properties. This viscoelastic model of ZP describes the viscous response of the porcine ZP under different indentation speeds of AFM tip (from 0.5 to 10 μm/s) that simulates spermatozoa with different velocities. "As the indentation rate increases, viscous effects dominate and neglecting them leads to significant errors" (Boccaccio et al., 2014; Papi et al., 2013).

None of the models investigate the frictional contact between the spermatozoa head and the ZP, neither the sperm impact angle on stress and deformation generated in the ZP during sperm penetration process. Furthermore, noted models do not consider impact of spermatozoa on the ZP surface.

Bedford (2006) examined the problem of why the penetrating sperm creates an oblique path in the ZP, as ultrastructural analysis of mammal ZP by transmission electronic microscopy showed that the spermatozoid ZP penetration path has an oblique form (Bedford, 1998). He also discussed the benefits of this path for the developing embryo: "A small radially directed hole enlarges significantly as the zona stretches and thins during expansion of the trophoblast, which then tends to protrude or herniate" (Bedford, 2006).

The goal of this study was to investigate the frictional contact between the spermatozoid head and the ZP, to test if sperm impact angle could influence the local contact dynamics in ZP and to test are there some sperm impact angles that are more favorable for sperm penetration.

2. Methods

2.1. Model description

The simulation was performed for mouse (*mus musuclus*) sperm–oocyte interaction for in vitro conditions at 37 °C (mouse body temperature) (Rhodes et al., 2000), www.schools.nsw.edu.au/animalsinschools/index.htm. For in vitro conditions an oocyte/s and certain amount of spermatozoa are in liquid medium in petry dish. Govern by chemotactical, and rheotactical factor spermatozoa swim freely in direction to oocyte. Model consists of an oocyte bonded to a glass body and approaching spermatozoa. The glass body mimics the petry dish and prevents the oocyte movement upon impact of spermatozoa. Mouse oocyte was modeled as a sphere that consists of three concentric asymmetric solid layers: ZP, perivitelin space and cytoplasm with nucleus. Each layer has different material properties. Dimensions of the mouse oocyte were taken from (Sun et al., 2003) – (52 µm-diameter of the oocyte, 4.5 µm-thickness of the ZP, diameter of the cytoplasm and nucleus was approximated on 33 µm). The asymmetry of the layers was taken for the following reason: in the process of fertilization, before the sperm cells reach the ZP of an oocyte, oocyte is in the metaphase-II (MII) stage of cell division and expels polar body in the perivitelin space. The polar body causes the position of the oocytes' cytoplasm and nucleus to be slightly asymmetric. Young modulus of mouse ZP (mZP) of an oocyte was taken from (Sun et al., 2003) – 17, 9 kPa.

Dimensions for mouse spermatozoa were taken from (Cummins and Woodall, 1985) for *mus musuclus* species: (sperm head length – 7.9 µm, sperm head width 3.2 µm, midpiece length 18.4 µm, midpiece width – 1.3 µm). In the model sperm head shape is in the form of an ellipsoid body. The sperm flagellum was not included in the model as it was assumed that the flagellum

contribution to overall spermatozoa mass could be neglected due to specific spermatozoa morphology. Majority of the spermatozoa mass is concentrated into the spermatozoa head and whole mass of the single spermatozoa is very small-order of magnitude 10^{-14} kg Spermatozoa impacts ZP surface under certain angle α (Fig. 1a). Sperm approaching velocity was taken as strait line velocity of progressive mouse sperm approximated on 100 µm/s (Goodson et al., 2011). Unlike the model of Kozlovsky and Gefen (2013), this model includes the moment of sperm impact on the ZP.

The finite element analysis is done using a commercially available software package ANSYS WORKBENCH version 14.5, as a transient structural analysis. The model geometry was defined in AUTODESK INVENTOR software package. As the observed model is symmetric in regard to geometry and boundary conditions, only one half of the model was considered. All model components were meshed using ANSYS SOLID187 element as a higher order 3-D, 10-node element (ANSYS 14.5 User Manual) Finite element mesh is shown on Fig. 1b. The properties of materials used in analysis at reference temperature of 37 °C are shown in Table 1. (taken from Hedrih and Ugrcic (2012)). It was assumed that all materials exhibit linear elastic behavior.

To increase the accuracy of FE computations the expected zone of spermatozoa impact, as well as the spermatozoa head, were meshed with a higher density mesh as shown on Fig. 2. The zone of the high quality mesh was positioned according to the expected impact point, with the change of the approaching angle (Figs. 1b, and 2). The total number of elements of the finite element model varies for different impact angles between 55,813 and 62,092. The

Table 1
The properties of materials used in analysis at temperature of 37 °C (from Hedrih and Ugrcic (2012)).

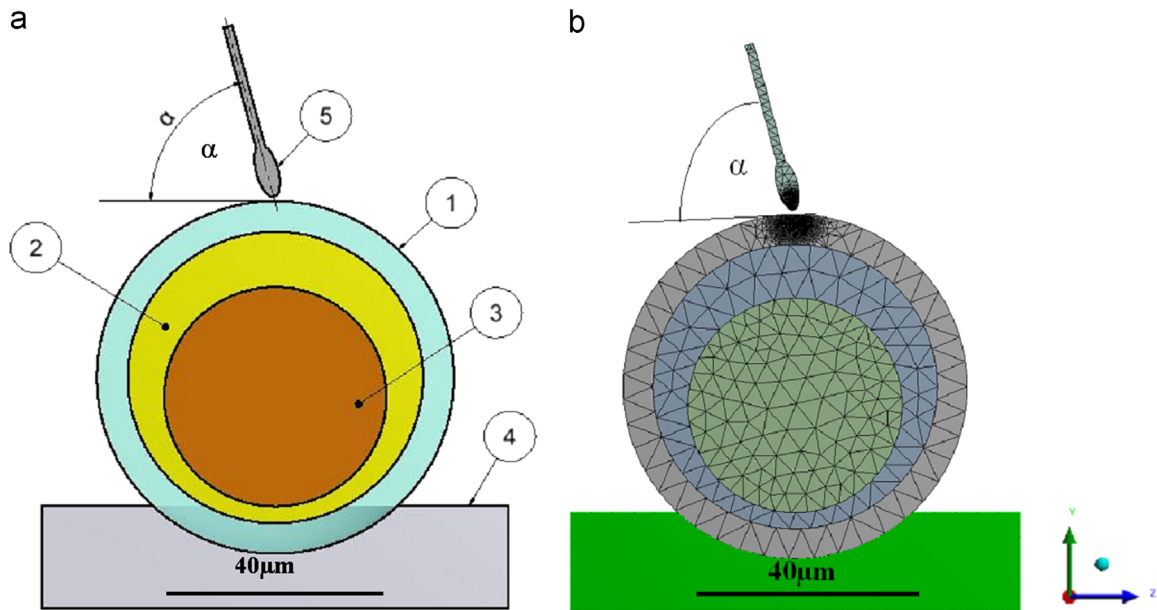| Material	Density (Kg/m³)	Young's modulus (Pa)	Poisson's ratio
ZP	1005	17,900	0.499
Perivitelin space	1013	17,200	0.490
Nucleus with cytoplasms	1040	7200	0.250
Glass	2530	5.448E+7	0.300

Fig. 1. (a) Components of the model: 1. ZP, 2. perivitelline space, 3. cytoplasm with nucleus, 4. fixed support, 5. sperm impact angle α. (b) Finite elements mesh in the axial cross-section of the sperm–oocyte contact model.
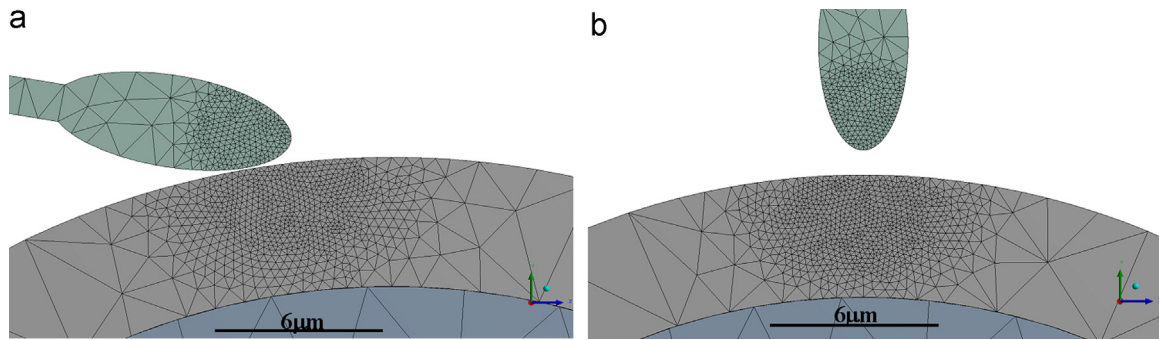
Fig. 2. Details of finite elements mesh in cross-section of the model for sperm impact angle α: (a)10°. (b) 90°.
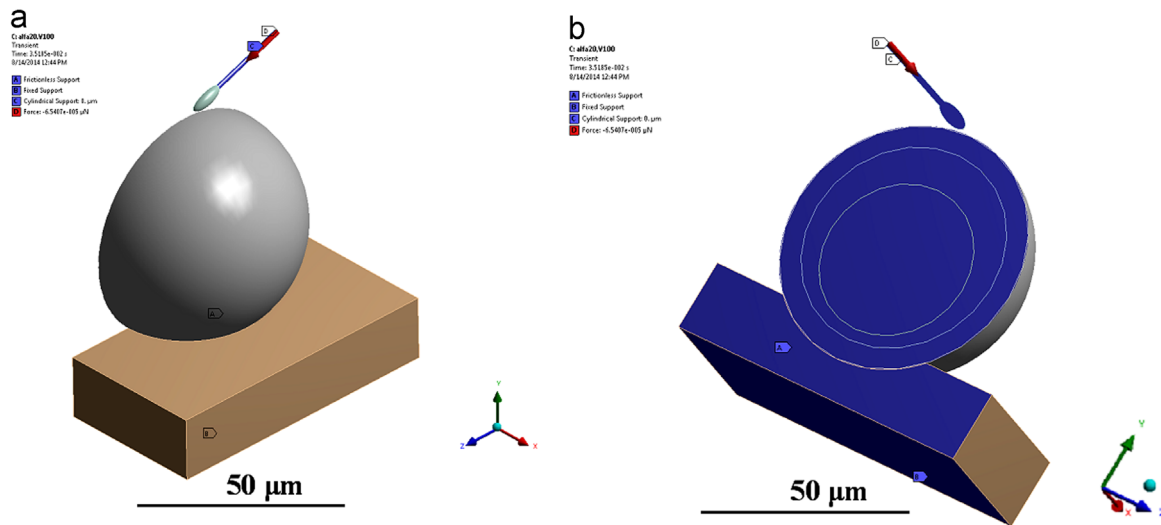

Fig. 3. Loads and boundary conditions of the model.

difference in element count is a consequence of positioning of the impact area.

The contact between the spermatozoid and the ZP was defined as a frictional, with the friction coefficient value of $\mu_f = 0.045$ (Angelini et al., 2012). The contact was modeled via the ANSYS CONTA174 and TARGE170 elements (ANSYS 14.5 Help) that correspond to spermatozoid, as a contact surface, and ZP, as a target surface. To facilitate the convergence due to non-linear contact definition, the contact was treated as a symmetric pair. During simulation the augmented Lagrange formulation was adopted. The contact stiffness was updated in every solution iteration automatically.

A mesh size sensitivity test was performed for the case of impact angle of 10° to obtain confidence in accuracy finite element simulations. It was assumed that the simulation results are insensitive to mesh size if the difference in equivalent stress and total deformation in two adjunct meshes is below 5%.

Density of the perivitelline space was approximate to density of cytoplasm and density of nucleus with cytoplasm together to density of nucleus.

The loads and boundary conditions are shown in Fig. 3. As only one half of the model was considered a frictionless support was inserted at the symmetry plane. The cylindrical part of spermatozoid midpiece was constrained via the axially free cylindrical support to ensure straight line travel of spermatozoa till the impact point and aid the convergence of the solution. It was necessary to constrain the spermatozoa to obtain convergence of the solution due to unpredictable spermatozoa motion upon impact in case of no support. The holder was constrained via the fixed support. Spermatozoa velocity was defined via the initial conditions. The simulation was performed in two steps: in the first step the spermatozoa travels with constant velocity till the oocyte until the contact with the ZP. Time of spermatozoa–ZP contact was determined with resolution of 1-e5 s. From the time of contact (second step) penetration force starts to act on the ZP, linearly increasing its value to the maximum in time frame of 25 e-3 s, which correspond to experimental data as determined by Allen et al. (2010). Penetrating force was defined as:

$$P_{prop} = \frac{2\pi\mu L_f V}{\ln(L_f/3r)} \tag{1}$$

(proposed by Kozlovsky and Gefen (2012) by Green (1988)), where μ is the dynamic viscosity of the surrounding liquid medium, ($\mu = 0.001$ Pa · s), L_f is the length of the flagellum, (96.6 μm) r is the radius of the flagellum (1.3 μm) (Cummins and Woodall, 1985) and V is the velocity of the spermatozoa (taken as 100 μm/s) (Goodson et al., 2011). For details see (Kozlovsky and Gefen, 2012). The force was applied at the end of midpiece as the force generated by the flagellum (not modeled) transmits over the midpiece.

The analysis was performed with a fixed time step of 5e-4 s. It was determined that the selected time step is sufficient to obtain insensitivity of results (equivalent stress and total deformation) to time step size by selecting of a smaller step (1e-5) and performing the analysis for the angle of 10°.

The equations of dynamical equilibrium of the bodies in the contact for numerical procedure of solutions were solved with sparse equation solver and full Newton method for treating the

non-linear contact equations. Authors assumed large deformations and strains (large deflection option in ANSYS) as the non-linear solution is more accurate. Furthermore, the solution is already non-linear due to non-linear contact so there is no computational performance penalty.

Governing equations for the nonlinear analysis based on large deformation theory can be found in ANSYS 14.5 Help (Mechanical APDL Theory Reference).

3. Results and discussion

Mechanical impacts of spermatozoa on ZP that precludes to biochemical effects in combination with biochemical processes (enzyme lyses and binding to ZP glycoproteins) are required and contribute to sperm penetration.

Bedford research (Bedford, 1998) indicates that eutherian spermatozoa have evolved a new strategy for ZP penetration based on cutting thrust that appear to preclude a conventional lytic mode of its penetration. This strategy is developed as a response to the resilient elasticity and thickness of the ZP. From the bio-mechanical standpoint spermatozoa that could generate a maximum local stress in the ZP, has maximum penetration and better chance to fertilize the oocyte. Conditions under these events occur regarding sperm impact angle are presented below.

All the presented results, other than contact results (pressure, frictional stress and sliding distance) and spermatozoa penetration, were calculated automatically by ANSYS software. More info on procedures for calculation of reported results can be found in ANSYS 14.5 Help. As symmetric contact definition was used, the contact results were calculated as an average of results on the contact and target side. The spermatozoa penetration was considered as the directional deformation of ZP in the vertical direction.

Maximum local equivalent stress, maximum contact pressure, total contact stress and frictional stress in local contact zone on ZP generated by impact of spermatozoa, were found to be dependent of sperm impact angle (Fig. 4). In Fig. 4 non-linear relation between noted parameters and sperm impact angle on tangent plane of ZP is notable. There are local minimums and local maximums of maximum equivalent ZP stress (MES), maximum contact pressure, total contact stress and frictional stress for certain sperm impact angles.

Local maximums of MES loc$[\max \sigma_{equ\,max}]$ are for sperm impact angles α 40°, 60°, 75° respectively, with maximum value max $[\max \sigma_{equ\,max}]$ for sperm impact angle $\alpha = 75°$.

Local minimums of MES $-$loc$[\min \sigma_{equ\,max}]$ are for sperm impact angle α 10°, 30°, 50°, 70°, 90° with minimal value min $[\max \sigma_{equ\,max}]$ for $\alpha = 10°$.

Although it was expected that the maximum equivalent stress in local contact zone of ZP would be obtained for the angle of 90°, the simulation results showed otherwise. As already noted the maximum ZP equivalent stress is obtained for impact angle of 75° (Fig. 5) that can be explained by introduction of frictional forces between the spermatozoa head and ZP. The penetration force can be decomposed in two components: the first one is tangential force in contact surface direction and second one is radial force in perpendicular direction of the contact surface (Fig. 6).

Tangential component is equal to the sliding friction force that resists the spermatozoa head movement on the ZP surface. For sperm impact angle of 90° the frictional forces is minimal due to absence of tangential force component which causes sliding resistance, as only one force component exists – the radial one. However, at 90° the minimal friction force exists and it is caused by progression of contact from point to surface because of elastic deformation of sperm head and ZP. The maximum equivalent stress in local contact zone on ZP for sperm impact angle of 75° corresponds to previous research, as Hedrih et al found, by usage of oscillatory spherical net model of mouse ZP (unpublished data), that for noted angle there is a local maximum of amplitudes of knot molecules movements (displacements) in the ZP net model. For sperm impact angle 75° MES has its maximum while contact pressure, frictional stress and total contact stress of ZP have their maximum values (Fig. 4). One can conclude that, from mechanical standpoint, sperm impact angle of 75° is favorable for penetration through ZP.

Analysis of propulsive force change for different sperm impact angles at the beginning of the contact at one contact point into ZP uses elements of mathematical phenomenology of mechanism of contact dynamics between spermatozoa and oocyte, spermatozoa's penetration and local ZP stress (Petrovic, 1911). The resultant equivalent stress in ZP is a result of radial and tangential component. Radial component depends on propulsive forces and tangential force component depends on propulsive force, sperm-impact angle and combination of kinetic and static friction coefficient. As sperm-impact angle is getting wider, resultant radial component is getting higher according to the sinus low: $F_{nr} = F_{prop} \sin \alpha$, and resultant tangential component is result of subtraction of tangential component of propulsive force F_t:

$$F_t = F_{prop} \cos \alpha \tag{2}$$

and friction force F_μ:

$$F_\mu = \mu_f F_n = \mu_f F_{prop} \sin \alpha = F_{prop} \sin \alpha \, tg\gamma \tag{3}$$

where γ is friction angle and μ is friction coefficient $\mu_f = tg\gamma$.

Resultant force in tangent direction is in the form:

$$F_{tr} = F \frac{\cos(\alpha+\gamma)}{\cos \gamma} \tag{4}$$

Resultant maximum local equivalent stress in the zone around impact point/zone of ZP is result of superpositioning of stress caused by normal component of force, that changes according to the sinus low of angle α and resultant tangential force of sperm that change according to the $\frac{\cos(\alpha+\gamma)}{\cos \gamma}$ rule. In Fig. 6 forces acting on the ZP surface regarding different sperm impact angles are defined.
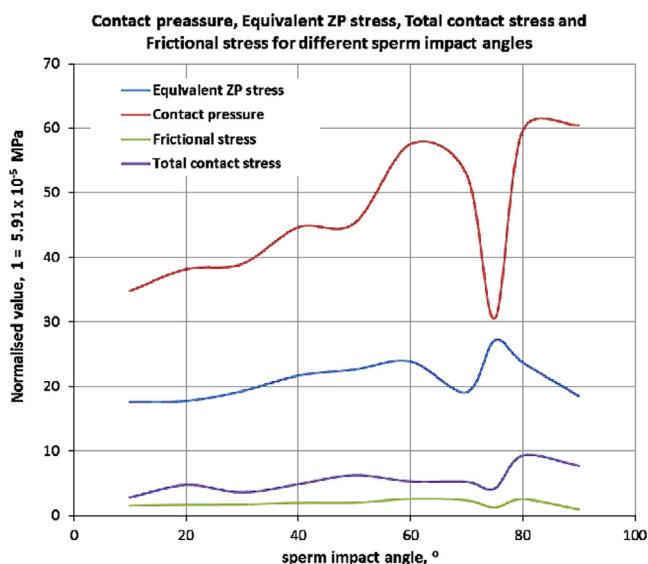

Fig. 4. Contact pressure, maximum equivalent ZP stress, total contact stress and Frictional stress regarding different sperm impact angles.
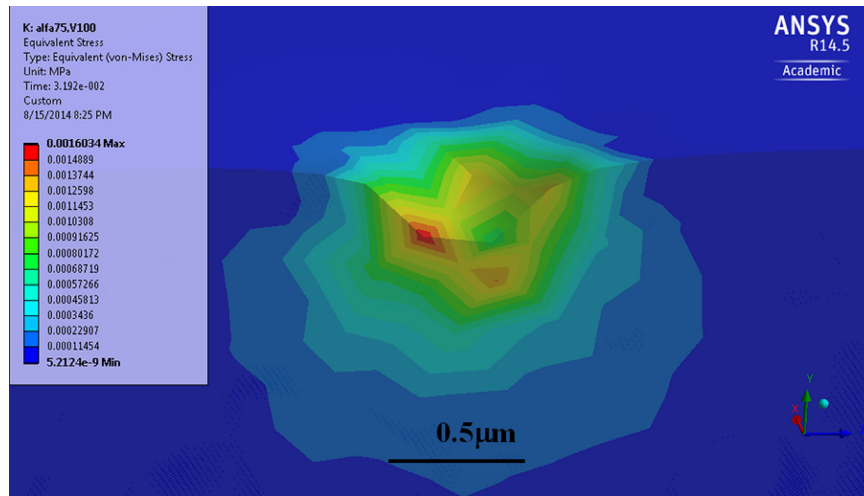
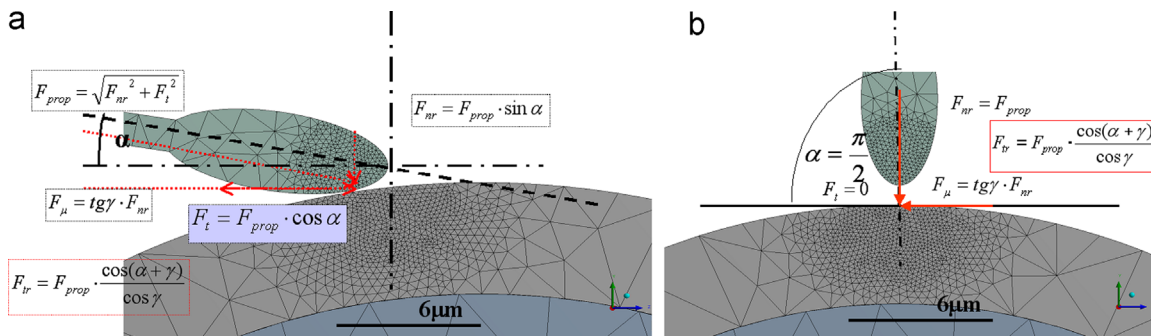**Fig. 5.** Maximum equivalent stress at ZP obtained at $\alpha=75°$.

Fig. 6. Schematic presentation of forces acting at sperm–oocyte contact for different sperm impact angles (a) 10° (b) 90°.
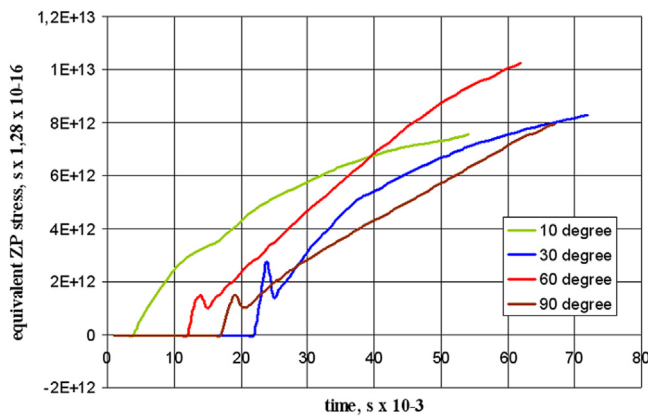

Fig. 7. Maximum equivalent stess in ZP over simulation time for different sperm impact angles.

Superpositioning of these forces could explain the maximum of MES for $\alpha=75°$.

Furthermore, it is observed during simulation that maximum equivalent stress of ZP is predominantly induced by spermatozoa propulsion (penetration) force. It is evident from Fig. 4 that the impact of spermatozoa to ZP causes equivalent stress that is significantly smaller than the one caused by propulsion (penetration) force. This can be explained by significantly lower mass of spermatozoa in comparison to oocyte. The obtained result suggests that even with higher impact velocity, as in case of hyperactivated spermatozoa, the sperm impact would generate equivalent stress that is smaller than the one generated by a penetration force. The noted remark should be tested with the higher impact velocities.

MES increases over time of the sperm–oocyte contact for all sperm impact angles reaching the maximum value at the end of simulation i.e when the penetration force reaches its maximum value (Fig. 7).

Contact pressure and Total contact stress exhibit the same trend regarding sperm impact angle (Fig. 4). Local maximums for both parameters are obtained for impact angles of 20°, 50° and 80°. Furthermore, there is an absolute maximum of contact pressure and total contact stress at impact angle of $\alpha=80°$. Local minimums for both parameters are at sperm impact angles 10°, 30°, 60°, 75°, 90° with minimal value at $\alpha=10°$.

Frictional stress exhibits local maximums are at $\alpha=20°$, 50°, 70°, 80°, with maximum value at $\alpha=80°$ and local minimums for α:10°, 30°, 60°, 75°, 90° of frictional stress can be identified with minimum value for $\alpha=90°$ (Fig. 8).

Fig. 9 shows the change of spermatozoa velocity during simulation. It is evident that spermatozoa impact the ZP with velocity that is defined by initial conditions. A different impact time is caused by different initial distance of spermatozoa from the ZP. After a very small drop of velocity, then for all cases the velocity increases due to the start of action of the spermatozoa propulsion (penetration) force in the form of impulse forces (Blehman et al., 2005). The differences in peak velocity value can be explained by a slight miss of exact impact time (impact time was determined with resolution of 1e-5 s). From the peak value the velocity than drops to the stable value. The time to stable velocity value is approximately one half of penetration force acting time i.e 12.5e-3 s. It is interesting to observe that for lower impact angles (below 30°) the stable velocity is between 5 and 10 µm/s which suggests that spermatozoa is still sliding on a ZP surface at the end of simulation. Furthermore, it is observed that there are oscillatory
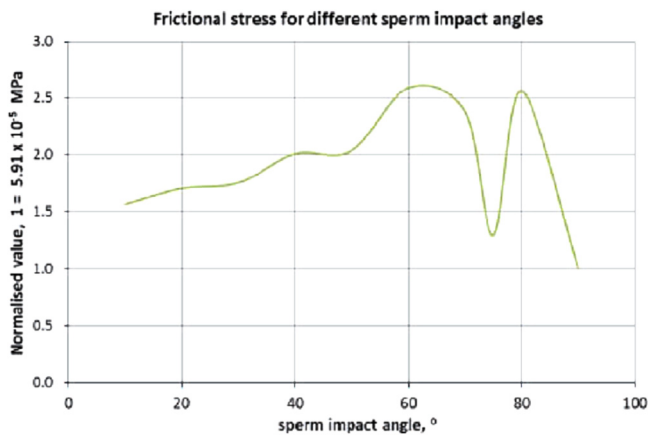
Fig. 8. Frictional stress at ZP membrane generated for different spermatozoa impact angles.
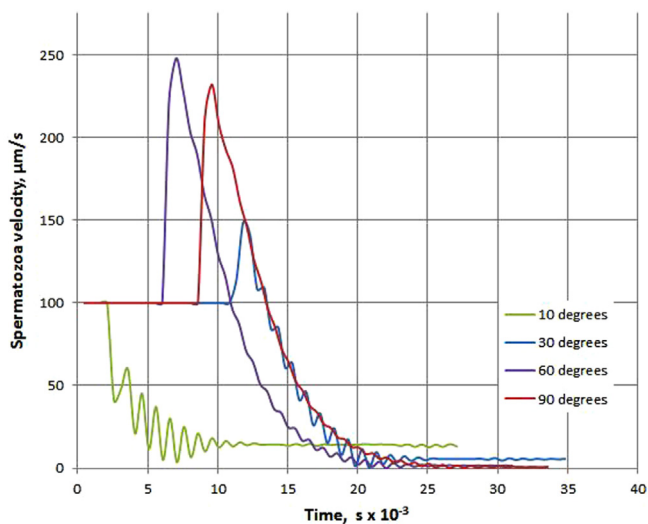

Fig. 9. Change of spermatozoa velocity during simulation time.

changes of spermatozoa velocity during a velocity drop phase suggesting that spermatozoa accelerates and decelerate during the sliding on the ZP surface which is characteristic to slip – stick motion. For sperm impact angle of 10° at the end of the simulation time, sperm velocity is higher then it is for sperm impact angles above 10° (30°, 60°, 90°).

It is consequence of sliding of spermatozoas' head on the ZP surface for the noted angle. Also the effect of slow sperm velocity, and spermatozoas' slow beating frequency (Ishijima, 2011; Gadella, 2013) duration of the sperm–oocyte contact, and larger contact area for sperm impact angle of 10° could contribute to receptor–recognition between spermatozoa and oocyte surfaces. It seems that lower sperm impact angle better preserves sperm energy during sperm–oocyte contact.

It is observed during review of simulation results that spermatozoa head exhibits motion which resembles slip-stick motion on the ZP surface due to low interface friction of living cells (Angelini et al., 2012) (friction coefficient between 0.03 and 0.06) (Fig. 10).

Reviewing of contact status over time (Fig. 10) is in agreement with diagram of sperm velocity change over time (Fig. 9). For a low impact angle of 10° the sperm head is constantly sliding over the ZP surface. For impact angle of 50° there are numerous changes between the sliding and sticking which imply the effect which resembles the slip-stick motion of spermatozoa head over the ZP surface. At impact angle of 90° the spermatozoa head is

predominately sticked to ZP surface. It is observed that motion of spermatozoa head that resembles slip – stick motion ocures between impact angles of 30° and 90°. In the noted interval the number of slip-stick changes decreases with the increase of impact angle.

The phenomenon of the slip-stick motion creates conditions for self-induced local relaxation oscillations on the basis of energy relaxation (Van der Pol, 1927; Cao, 2013).

In a time period of spermatozoa–ZP surface contact, spermatozoa gives mechanical energy of the impact to ZP. In the next time period accumulated mechanical energy is realized into slipping oscillatory relative motion of spermatozoa on ZP surface causing self-induced oscillations of relaxation to appear both in local area of the ZP and motion of the spermatozoa.

In this case self-induced relaxation oscillations in the ZP propagates trough ZP surface as surface waves. Due to small mass of spermatozoa head compare to mass of the ZP, spermatozoa could be considered as a digit-solid body that oscillate as a mass particle.

In interactions of these two self-induced oscillations caused by relaxation of accumulated energy a time period of possible spermatozoa propagation through ZP could be considered. These self-induced oscillations of relaxation could be important in interactions with biochemical and physico-chemical non-linear dynamical processes.

In approximation for describing this process of self-induced oscillations of relaxation qualitative analogy and phenomenological mapping of oscillations of relaxations that appear in motion of material particle on the spring by a rough track that moves with constant speed relative to material particle of the oscillator (Fig. 11). This kind of motion is described by non-linear Van der Pol differential Eqs. (5) and (6) with large parameter ε:

$$\frac{d^2x}{dt^2} + \varepsilon\left[\frac{dx}{dt} - \frac{1}{3}\left(\frac{dx}{dt}\right)^3\right] + x = 0 \tag{5}$$

or

$$\frac{d^2x}{dt^2} + \varepsilon f\left(\frac{dx}{dt}\right) + x = 0 \tag{6}$$

Sperm motion is analogue to motion of the mass particle on the spring (oscillator) that moves along rough surface of treadmill (corresponds to the surface of ZP (Familiari et al., 2006; Martinova et al., 2008) at the moment of ovulation (Murayama et al., 2006)). Treadmill is moving over rotating discs with constant velocity v_0. Velocity of sperm/an oscillator $\dot{x}$ is characterized with changing of its coordinates x and depends of rigidity of the spring k and treadmill velocity v_0 (Fig. 11a).

Elastic force acting on sperm/oscillator with mass m is in the form:

$$F_e = -kx \tag{7}$$

Frictional forces acting on sperm/oscillator moving along the rough surface of treadmill with velocity of v_0 depends of sperm/oscillator relative velocity $\dot{x} - v_0$:

$$F_{tr} = -F(\dot{x} - v_0) \tag{8}$$

Specific resistant force generated during motion of sperm/oscillator moving along the rough surface of treadmill (Van der Pol differential Eq. (5)) is:

$$-F(\dot{x}) = \varepsilon\left[\frac{dx}{dt} - \frac{1}{3}\left(\frac{dx}{dt}\right)^3\right] \tag{9}$$

dependant on cubic function of velocity. In general case it is in the form:

$$-F(\dot{x}) = \varepsilon f\left[\frac{dx}{dt}\right] \tag{10}$$
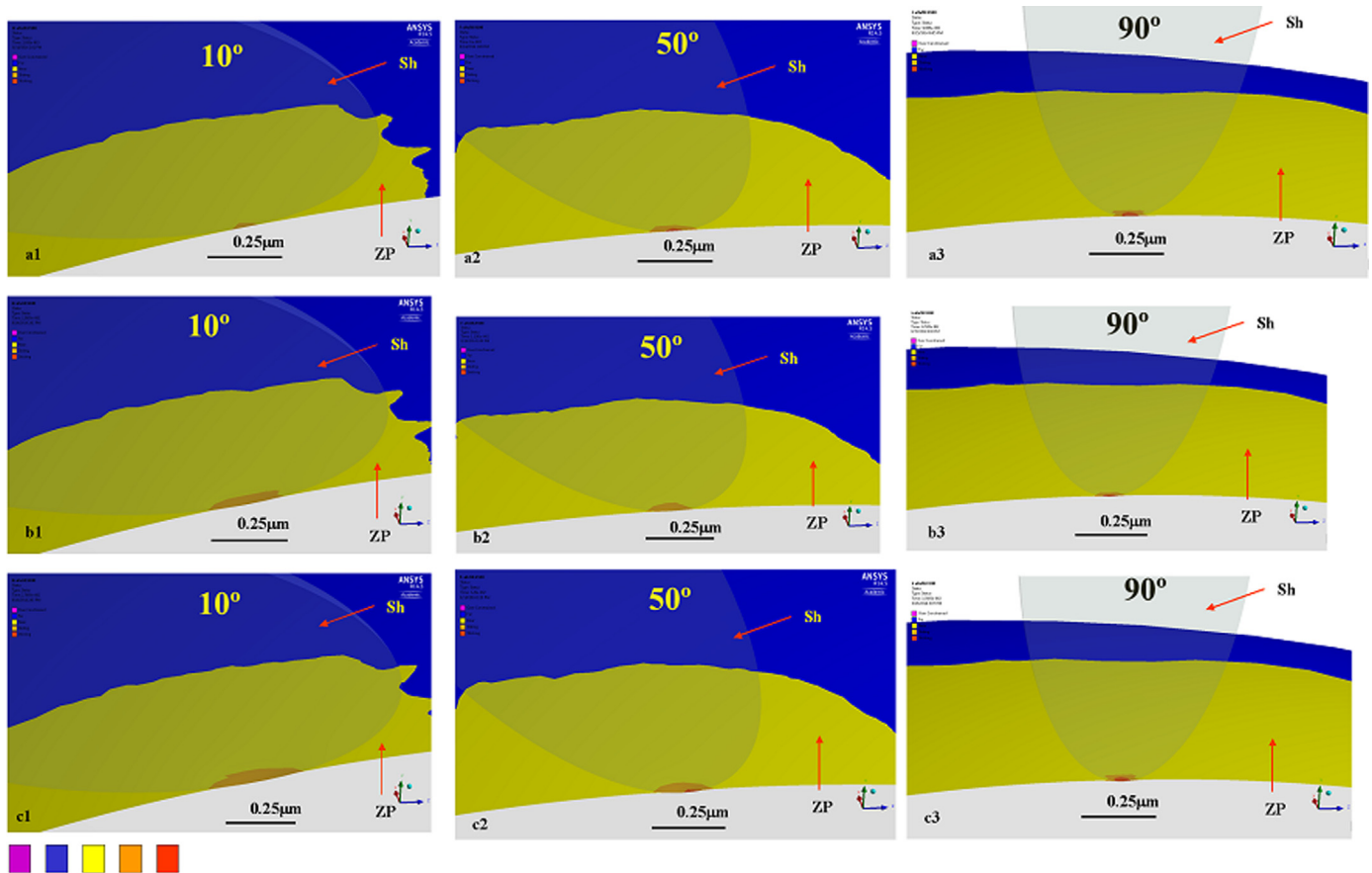
Fig. 10. Contact status for different sperm impact angles observed in different time points: a1-3 at the beginning of the contact. b1-3 and at the half-time point. c1-3 at the end of the simulation for different sperm impact angles a1,b1,c1 for 10°, a2,b2,c2 for 50° and a3,b3,c3 for 90°. Legend: violet—over constrained, blue—far, yellow—near, orange—sliding, red—sticking. (For interpretation of the references to color in this figure legend, the reader is referred to the web version of this article.)
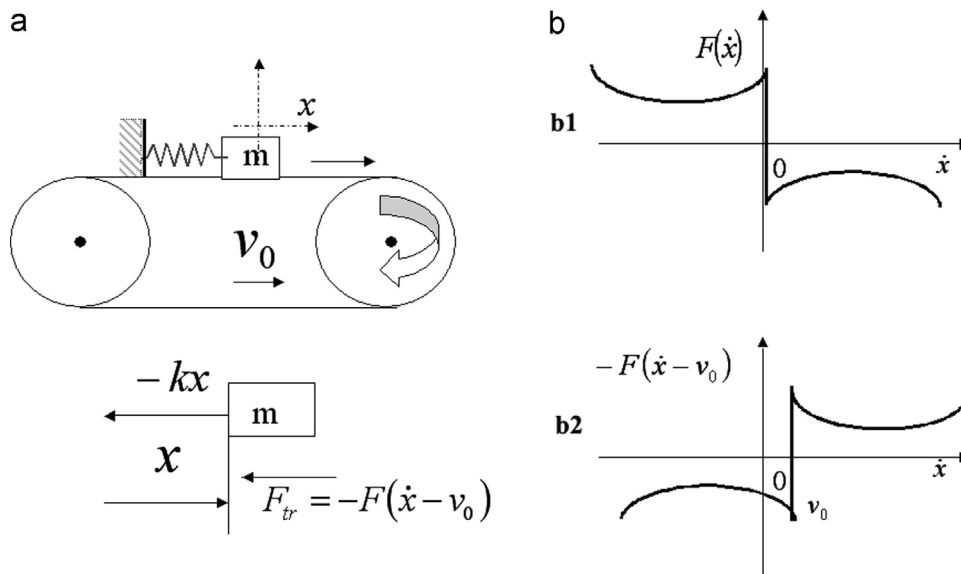

Fig. 11. a) Resistant forces acting on mass on a spring moving on the treadmill. b) Graphical presentation of dependence of frictional force and velocity of the mass when (b1) treadmill is not moving. (b2)Treadmill is moving with velocity v_0.

For the theoretical case when the sperm/oscillator is in peace diagram of resistant force has form like in Fig. 11b1. This theoretical case does not happen in reality in physiological conditions. When sperm/oscillator is moving, resistant force has diagram like on Fig. 11b2. This mathematical and mechanical phenomenology

corresponds to the time profiles of the sperm velocity obtained in our numerical experiment (see Fig. 9).

Fig. 9 shows notable phenomenon of relaxation oscillations where sperm velocity is increasing and decreasing on a specific manner. As kinetic energy depends of its velocity it seams like
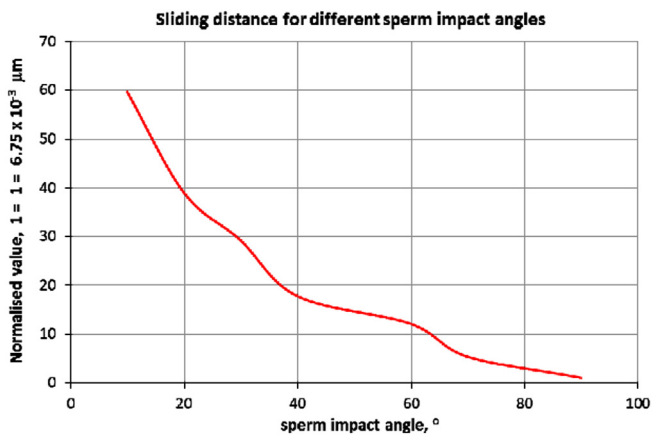
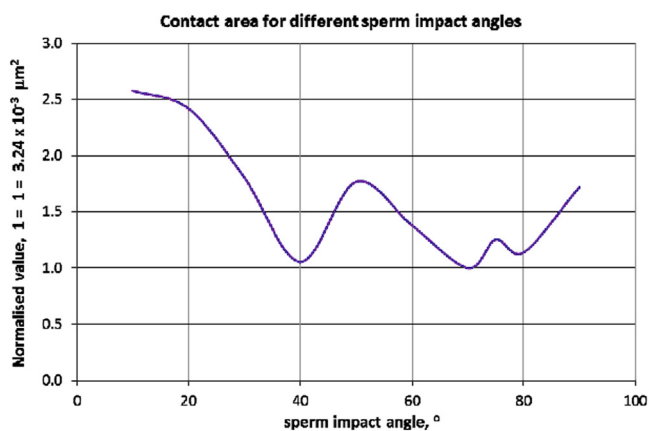**Fig. 12.** Sliding distance of sperm head for different sperm impact angles.

Fig. 14. Total deformation of ZP and Maximum penetration of ZP for different spermatozoa impact angles.

Fig. 13. Contact area of ZP for different sperm impact angles.

area as shown on Fig. 13. Contact area also exhibits local minimums (for $\alpha=10°$, $50°$, $75°$, $90°$) and local maximums (for $\alpha=40°,70°$, $80°$). Theoretically, larger contact area can ensure biologically better contact due to better sperm–oocyte recognition and receptor binding between sperm head and ZP surface enabling chemical modifications of ZP glycoproteins (Clark, 2011).

Fig. 14 shows the total deformation of ZP at the end of transient structural simulation. The sperm impact angles of 10° and 70°, 90° stand out as local maximums of total deformation and total propagation of spermatozoa head. Local minimums are at sperm impact angles 20°, 50°, 75°. Total ZP deformation and Maximum sperm penetration of ZP have almost the same trend.

From the Figs. 4 and 14 for sperm impact angle 75° there are maximum of MES and local maximum of contact area and local minimums for frictional stress, total contact stress, total deformation and maximum penetration. This combination of mechanical parameters could be optimal for initial sperm penetration into ZP.

Values of maximum obtained deformation in normal direction (penetration depth) are still much smaller compared to the total ZP thickness and multi-layer structure of ZP should not be neglected (Familiari et al., 2006; Martinova et al., 2008).

Findings presented in the paper and work by other authors suggest that contact between the spermatozoa and ZP is a specific tribological, biodynamical and physico-chemical system that should be further investigated especially for contact of viscoelastic/viscoplastic biodynamical and physic-chemical bodies.

This would be possible by using constitutive relations expressed by fractional order derivatives and also integral terms containing kernel of relaxation or kernel of retardation of biomaterial. In the real biological system ZP is multi-layer mesh-like structure. On scanning and transmission electron microscopy two basic ZP layers could be identified: outer with rough spongy appearance and inner with smaller fenestrations and smooth fibrous network (Martinova et al., 2008). After fertilization outer ZP showed rougher meshed network due to fusion between filaments as a consequence from sperm penetration while the inner was smoother with melted appearance (Martinova et al., 2008). "In both the inner and outer ZP layers, stiffness decreased at maturation while, conversely, increased after fertilization" (Papi et al., 2012). Morphological and structural changes of ZP after fertilization are followed by changes in its mechanical properties (Papi et al., 2009).

Boccaccio et al.'s (2012, 2014) FE model of ZP and our FE model are both appropriate although the approach and the assumptions are different. While Boccaccio et al. (2012, 2014) considering sperm–oocyte contact as frictionless we consider the sperm–ZP

(from Fig. 9 and mechanical analogy from Fig. 11) that sperm accumulates energy (when its velocity decreases may correspond to lower kinetic and higher potential energy) and then start to oscillate with higher speed (then its velocity increases-may correspond to higher kinetic energy) although sperm velocity has general toothed decline trend.

As resistant force dependent on cubic function of velocity (9) it follows that as sperm/oscillator velocity increases, the resistant force will increase much more. Similar experimental results were obtained by Papi et al. (2013) suggesting that, sperm develops a strategy to overcome this ZP reaction decreasing its velocity over time. In experiments of Papi et al. (2013) higher force (in the form of AFM tip) applied to the ZP surface produces higher ZP reaction and lower indentation of ZP. Force exerts by AFM probe to the ZP simulates the interaction of spermatozoa and ZP. According to Papi et al. (2013) this effect is the result of viso-elastic properties of ZP. ***This complex phenomenon of slip-stick generated in the first moment of sperm impact on ZP in combination with specific decreasing of its velocity over time sheds new light on mechanical component of sperm–ZP contact.

The diagram of sliding distance (Fig. 12) revels maximum sliding at sperm impact angle $\alpha=10°$ and minimum sliding distance for impact angle $\alpha=90°$. Sliding of the spermatozoa head over ZP surfaces for impact angle of 10° is expected, as the geometry of the spermatozoa head at this impact angle provides favorable conditions for sliding in the low friction scenario.

The geometry of the spermatozoa head and the sperm impact angle have a significant effect on the non-linear contact between spermatozoa head and ZP surface and affect the size of contact
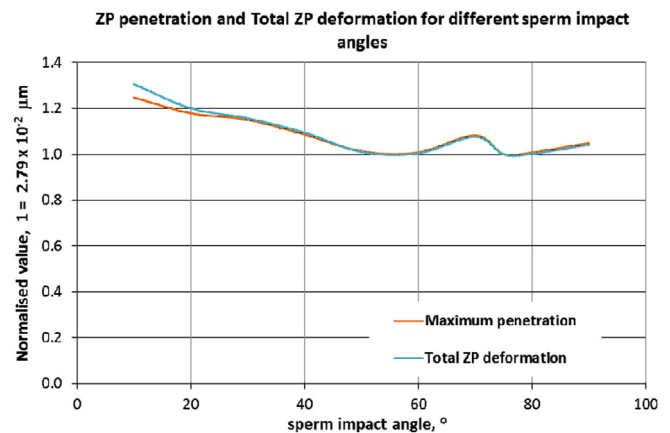
contact as a frictional one. We assume ZP as an elastic body, while they assume it has hyperelastic (2012) or viscoelastic properties (2014).

We were interested in the effect of friction and impact angle on the spermatozoa–oocyte local contact dynamics. The sperm–oocyte contact in our experiments was defined as non-linear frictional contact, which is one step forward. The Boccaccio et al.'s (2012, 2014) models are adequate for AFM probing experiments on isolated ZP and examined issues. This models and approaches could not be compared in sense that one is better form another because they study different issues and both of them have their strengths. Neither of the FE models deal with relation between chemical reactions nor biomechanical events in sperm–oocyte contact mostly because the modeling parameters needed are still lacking. Some FE modeling of sperm (head was assume as a sphere) and its motility related to sperm angle near oocytes and spheres are described in (Ishimoto et al., 2015).

To model sperm interaction with ZP and consequent penetration the more complex model should be made–model that include nonlinear visco-plastic properties and multilayer structure of ZP.

3.1. Limitation of the model

For the simplicity of the model, rotational speed of a sperm cell was not included. This rotational speed is also important for fertilization (Subramani et al., 2014; Gaffney et al., 2011) and sperm–ZP dynamics. Furthermore, ZP was modeled as ideally elastic structure which is not case in reality as noted tissues exhibit viscoelastic behaviour. For the simplicity of the model, only impact of one spermatozoa was considered. In real biological situation one spermatozoa is not enough for fertilization. The conjoint actions of many spermatozoids are required. In biological system many spermatozoa (in range 10^6) are impacting the ZP surface. Furthermore existence of coupled fields (mechanical, electrical chemical) should be considered. In paper of Allena and Aubry (2011) coupling between electricity, geometry and mechanics was used for parameterizations of shell-like deformations inside biological membranes. Although this technique was used for modeling the deformations of the membrane of the Drosofila embryo, we are of opinion that this technique could be used for deformations of the ZP in process of fertilization.

This paper did not concern the biomechanical effects in sperm head. The FE analysis of stress and strain in sperm head during frictional contact with oocyte would be also an important subject for studying specially from the aspect of the angle. Many questions regarding sperm–oocyte dynamics are sill opened. For example what would be the angle that would contribute enough to acrosom reaction to occur? Coupling biomechanical and chemical effect is a great problem because of lacking the adequate parameters that should be input in to the model. To be more close to the answer careful and extensive research are needed and different approach to the problem. Regarding an potentially adequate approach one of the promising approach could be to treat the ZP as responsive polymer–polymer that respond to mechanical stimuli by oscillations in chemical reactions at principal that is similar to the principle describe in paper of (Yashin et al., 2012).

4. Conclusion

In this paper a biomechanical approach and FEM analysis were used to study local contact dynamic of sperm–oocyte interaction relative to different sperm impact angles. The sperm–oocyte contact was defined as non-linear frictional contact. From the obtained analysis we can conclude the following:

1. Non-linear frictional contact of ZP and spermatozoa has significant effect on spermatozoa–oocyte interaction dynamics (local maximum equivalent stress, local maximum deformation, sperm penetration)
2. Sperm impact angles under which maximum local deformation, maximum equivalent stress, maximum contact pressure, maximum frictional stress, maximum contact ZP area, maximum sliding distance and maximum sperm penetration are occurred are identified
3. Spermatozoa with sperm impact angle $\alpha = 75°$ achieves local maximum equivalent stress in ZP and has maximum contact area.
4. Spermatozoa with sperm impact angle $\alpha = 10°$ achieves maximum total deformation, frictional stress and sliding distance
5. Slip-stick effect and appearance of the self-induced oscillation of relaxation is identified as possible process favorable for next phase after impact to ZP for proceeding spermatozoa penetration using oscillations of the relaxation caused by vibrorheological effects and alternatively as effect of accumulation and relaxation caused by mechanical energy introduced in the system by sperm impact and sperm propulsion force.

Our further investigations should concentrate on the previously mentioned limitations of the model.

References

Allen, M.J., Rudd, R.E., McElfresh, M.W., Balhorn, R., 2010. Time-dependent measure of a nanoscale force-pulse driven by the axonemal dynein motors in individual live sperm cells. Nanomed.: Nanotechnol. Biol. Med. 6, 510–515.

Allena, R., Mouronval, A.-S., Aubry, D., 2010. Simulation of multiple morphogenetic movements in the Drosophila embryo by a single 3D finite element model. JMBBM 3, 313–323.

Allena, R., Aubry, D., 2011. A novel technique to parametrize shell-like deformations inside biological membranes. Comput. Mech. 47, 409–423. http://dx.doi.org/10.1007/s00466-010-0551-8.

Angelini, T.E., Dunn, A.C., Uruen, J.M., Dickrell, D.J., Burris, D.L., Sawyer, W.G., 2012. Cell friction. Faraday Discuss. 156 (31–39), 31.

Anderson, M.J., Dixson, A.F., 2002. Sperm competition, motility and the midpiece in primates. Nature Brief Commun. 416, 496.

Bedford, J.M., 1998. Mammalian fertilization misread? Sperm penetration of the eutherian Zona Pellucida is unlikely to be a lytic event. Biol. Reprod. 59, 1275–1287.

Bedford, J.M., 2006. Why do penetrating sperm create an oblique path in the zona pellucida? Reproduction 131, 23–25.

BlehmanII, J.M., Mischkis, A.D., Panovko, Y.G., 2005. Applied Mathematics-Subject-Logic, Particular Paroxysm, Mechanical Examples (In russian), 7. URSS, Moskva, p. 376.

Boccaccio, A., Frassanito, C.M., Lamberti, L., Brunelli, R., Maulucci, G., Monaci, M., Papi, M., Carmine, P., Parasassi, T., Sylla, L., Ursini, F., De Spirito, M., 2012. Nanoscale characterization of the biomechanical hardening of bovine zona pellucida. J. R. Soc. Interface 9, 2871–2882. http://dx.doi.org/10.1098/rsif.2012.0269.

Boccaccio, A., Lamberti, L., Papi, M., De Spirito, M., Douet, C., Goudet, G., Papalettere, C., 2014. A hybrid characterization framework to determine the viscohyperelastic properties of a porcine zona pellucida. Interface Focus 4, 20130066. http://dx.doi.org/10.1098/rsfs.2013.0066.

Cao, W., 2013. Van der Pol Oscillator. Celestial mechanics, MAT983. Junior Seminar on Hamiltonian Mechanics, p. 9.

Clark, G.F., 2011. The molecular basis of mouse sperm–zona pellucida binding: a still unresolved issue in developmental biology. Reproduction 142, 377–381.

Cummins, J.M., Woodall, P.F., 1985. On mammalian sperm dimensions. J. Reprod. Fertil. 75, 153–175.

Eisenbach, M., 1999. Mammalian sperm chemotaxis and its association with capacitation. Dev. Genet. 25 (2), 87–94.

Familiari, G., Relucenti, M., Heyn, R., et al., 2006. Three-dimensional structure of the Zona Pellucida at ovulation. Microsc. Res. Tech. 69, 415–426.

Firman, R.C., Simmons, L.W., 2010. Sperm midpiece length predicts sperm swimming velocity in house mice. Biol. Lett. 6, 513–516.

Flesch, F.M., Gadella, M.B., 2000. Dynamics of the mammalian sperm plasma membrane in the process of fertilization. Biochim. Biophys. Acta 1469, 197–235.

Gadella, B.M., 2013. Dynamic regulation of sperm interactions with the zona pellucida prior to and after fertilisation. Reprod. Fertil. Dev. 25 (1), 26–37.

Gaffney, E.A., Gadel, H., Smith, D.J., Blake, J.R., Kirkman-Brown, J.C., 2011. Mammalian sperm motility: observation and theory. Annu. Rev. Fluid Mech. 43, 501–528. http://dx.doi.org/10.1146/annurev-fluid-121108-145442.

Gefen, A., 2010. The relationship between sperm velocity and pressures applied to the Zona Pellucida during early sperm–oocyte penetration. J. Biomech. Eng. 132 124501-124501.

Goodson, S.G., et al., 2011. Classification of mouse sperm motility patterns using an automated multiclass support vector machines model. Biol. Reprod. 84 (6), 1207–1215.

Green, D.L., 1988. Sperm thrusts and the problem of penetration. Biol. Rev. 63, 79–105.

Hedrih, A., (Stevanovic) Hedrih, K., Bugarski, B., 2013. Oscillatory Spherical net model of Mouse Zona Pellucida. J. Appl. Math. Bioinform. 4 (3), 225–268.

Hedrih, A., Lazarevic, M., Mitrovic-Jovanovic, A., 2015. Influence of sperm impact angle on successful fertilization through mZP oscillatory spherical net model. Comput. Biol. Med. Comput. Biol. Med. 59, 19–29.

Hedrih, A., Ugrcic, M., 2012. Vibrational properties characterization of mouse embryo during microinjection. Theor. Appl. Mech. 40 (S1), 189–202, UDC 519.673:531:01.

Hedrih, A., Ugrcic, M. 2013. The use of finite elements method in vibration properties characterization of mouse embryo. In: Proceedings of Symposium Nonlinear Dynamics with Multy- and Inter-disciplinary Applications (SNDMIA 2012), Belgrade, October 1–5th 2012 (Eight Serbian Symposium in area of Nonlinear Sciences) A-01:1-15. Scientific review. Series: Scientific and Engineering Editor-in-Chief: Perović, S., Serbian Scientific Society, pp. 245–254. UDK 001 YU ISSN 0350-2910.

Ishijima, S., 2011. Dynamics of flagellar force generated by a hyperactivated spermatozoon. Reproduction 142, 409–415.

Ishimoto, K., et al., 2015. A simulation study of sperm motility hydrodynamics near fish eggs and spheres. J. Theor. Biol. http://dx.doi.org/10.1016/j.jtbi.2015.10.013i.

Kozlovsky, P., Gefen, A., 2012. The relative contributions of propulsive forces and receptor–ligand binding forces during early contact between spermatozoa and zona pellucida of oocytes. J. Theor. Biol. 294, 139–143.

Kozlovsky, P., Gefen, A., 2013. Sperm penetration to the zona pellucida of an oocyte: a computational model incorporating acrosome reaction. Comput. Methods Biomech. Biomed. Eng. 16 (10), 7.

Malo, A.F., Gomendio, M., Garde, J., et al., 2006. Sperm design and sperm function. Biol. Lett. 2, 246–249. http://dx.doi.org/10.1098/rsbl.2006.0449.

Martinova, Y., Petrov, M., Mollova, M., Rashev, R., Ivanova, M., 2008. Ultrastructural study of cat zona pellucida during oocyte maturation and fertilization. Anim. Reprod. Sci. 108, 425–434.

Miki, K., Clapham, D.E., 2013. Rheotaxis guides mammalian sperm. Curr. Biol. 23 (6), 443–452.

Murayama, Y., Mizuno, J., Kamakura, H., et al., 2006. Mouse zona pellucida dynamically changes its elasticity during oocyte maturation, fertilization and early embryo development. Hum. Cell 19, 119–125.

Nasseri, S., Phan-Thien, N., 1997a. Modelling micromachines with elastic parts in a viscous environment. Comput. Mech. 20, 242–246.

Nasseri, S., Phan-Thien, N., 1997b. Geometric optimisation of a micromachine with a spiral tail immersed in viscous medium. Comput. Mech. 20, 267–271.

Okabea, M., Cummins, J.M., 2007. Mechanisms of sperm-egg interactions emerging from gene-manipulated animals. Cell. Mol. Life Sci. 64, 1945–1958 1420-682X/07/151945-14.

Papi, M., Sylla, L., Parasassi, T., et al., 2009. Evidence of elastic to plastic transition in the zona pellucida of oocytes using atomic force spectroscopy. Appl. Phys. Lett. 94, 153902.

Papi, M., Brunelli, R., Familiari, G., et al., 2012. Whole-depth change in bovine zona pellucida biomechanics after fertilization: how relevant in hindering polyspermy? PLoS One 7 (9), e45696. http://dx.doi.org/10.1371/journal.pone.0045696.

Papi, M., Maiorana, A., C, Douet, C., et al., 2013. Viscous forces are predominant in the zona pellucida mechanical resistance. Appl Phys. Lett. 102, 043703–043705.

Petrovic, M., 1911. Elementi matematičke fenomenologije (elements of mathematical phenomenology). Srp. Kralj. Akad. Beogr., 89 http://elibrary.matf.bg.ac.rs/handle/123456789/476?locale-attribute=sr.

Rhodes, J.S., Koteja, P., Swallow, J.G., Carter, P.A., Garland, T.Jr, 2000. Body temperatures of house mice artificially selected for high voluntary wheel-running behavior: repeatability and e€ect of genetic selection. J. Therm. Biol. 25, 391–400.

Subramani, E., Basu, H., Thangaraju, S., Dandekar, S., Mathur, D., Chaudhury, K., 2014. Rotational Dynamics of Optically Trapped Human Spermatozoa. Scientific World Journal. http://dx.doi.org/10.1155/214/154367, Article ID 154367, 7 pages.

Sun, Y., Wan, K.T., Roberts, K.P., Bischof, J.C., Nelson, B.J., 2003. Mechanical property characterization of mouse zona pellucida. IEEE Trans. Nanobiosci. 2 (4), 279–286.

Talbot, P., Shur, B.D., Myles, D.G., 2003. Cell adhesion and fertilization: steps in oocyte transport, sperm-zona pellucida interactions, and sperm-egg fusion. Biol. Reprod. 68, 1–9.

Tourmente, M., Gomendio, M., Roldan, E.R.S., 2011. Sperm competition and the evolution of sperm design in mammals. BMC Evol. Biol. 11, 12. http://dx.doi.org/10.1186/1471-2148-11-12.

Yashin, V.V., Kuksenok, O., Dayal, P., Balazs, C.A., 2012. Mechano-chemical oscillations and waves in reactive gels. Rep. Prog. Phys. 75 (066601), 40. http://dx.doi.org/10.1088/0034-4885/75/6/066601.

Van der Pol, B., 1927. On relaxation-oscillations. Lond. Edinb. Dublin Phil. Mag. J. Sci. 2 (7), 978–992.